Supporting Information

Maestre-Reyna et al. 10.1073/pnas.1207653109

SI Methods

Yeast Strains. Yeast strains used in this study are described in Table S3. For isolation of the *EPAA* domains the *Candida glabrata* stain ATCC2001 was used. In vivo adhesion assays were performed in the nonadhesive *Saccharomyces cerevisiae* strain BY4741 carrying appropriate plasmids (Table S5). Standard methods for yeast culture medium and transformation were used as described in ref. 1.

Plasmid Construction. All plasmids used in this study are listed in Table S4. Numbering of amino acid residues refers to sequences described in the UniProt database (www.uniprot.org). BHUM1829 was obtained by PCR amplification of the *EPA1A* domain from genomic DNA of *C. glabrata* strain ATCC2001, using primers fwd-Epa1-aa31 and rev-Epa1-aa271, and subsequent insertion of the resulting XhoI/NdeI fragment into the vector pET-28a(+). BHUM1804, BHUM1805, and BHUM1806, carrying variants of the *EPA1A* domain with exchanged amino acid in CBL2, were generated via site-directed mutagenesis, using primers pET28_Epa1→6A Fwd and Rev, pET28_Epa1→2A Fwd and Rev, pET28_Epa1→3A Fwd_1 and Rev_1, and pET28_Epa1→3A Fwd_2 and Rev_2 and BHUM1829 as a template. To generate BHUM1835, BHUM1836, BHUM1889, and BHUM1892, the corresponding *EPA1A* domains were amplified using primers Epa_1.2_SacII and Epa_1.2_SacI together with BHUM1804, BHUM1805, BHUM1806, or BHUM1829 as a template and subsequent cloning of the resulting SacII/SacI fragments into BHUM1760. To obtain BHUM1983, BHUM1984, BHUM2016, and BHUM2017, the corresponding *EPA1A* domains including the *FLO11* secretion signal and the *3HA*-tag were amplified using primers SalI-SS-3HA-EpaXA and Epa_1.2-SacI together with BHUM1835, BHUM1836, BHUM1889, or BHUM1892 as a template and subsequent insertion of the resulting SalI/SacI fragments into BHUM1964. For the construction of BHUM1871 and BHUM1877, *EPA2A* and *EPA6A* wild-type domains were amplified using either primers Epa_2_SacII and Epa_2_SacI or Epa_6,7_SacII and Epa_6,7_SacI as well as genomic DNA from *C. glabrata* strain ATCC2001 as a template. The resulting SacII/SacI fragments were then inserted into BHUM1760. For the construction of BHUM1990, the *EPA3A* wild-type domain was amplified using primers Epa_3.2_SacII and Epa_3_SacI together with genomic DNA from *C. glabrata* strain ATCC2001 as a template. The resulting SacII/SacI fragment was then inserted into BHUM1964. To construct plasmids BHUM1985 and BHUM2018, DNA fragments were PCR amplified from plasmids BHUM1871 and BHUM1877, using primers SalI-SS-3HA-EpaXA together with either Epa_2-SacI or Epa_6,7_SacI, respectively. Resulting fragments carrying *3HA*-tagged versions of the *EPAA* domains were subsequently cloned into BHUM1964, using restriction enzymes SalI and SacI. BHUM1760 carrying (*i*) the *FLO11* promoter, (*ii*) the *FLO11* secretion signal spanning amino acid residues 1–30, (*iii*) the *FLO11BC* domain encompassing amino acids 214–1,360, and (*iv*) the *FLO11* terminator was generated by whole-vector PCR, using primers 1601-A2-SacI-SacII and Flo11-5 together with BHUM1601 as a template and subsequent ligation. BHUM1601 was obtained by PCR amplification of the *FLO11* genomic region from *S. cerevisiae* strain WY423, using primers HUM193 and HUM194 and subsequent cloning into the XbaI/XhoI-digested backbone of BHUM778 by homologous recombination in *S. cerevisiae* strain RH2662. BHUM1964 carrying (*i*) the *PGK1* promoter, (*ii*) the *FLO11* secretion signal covering amino acids 1–25, (*iii*) the *FLO11BC* domain spanning amino acid residues 214–1,360, and (*iv*) the *FLO11* terminator was constructed by replacing the *FLO11* promoter in BHUM1327 with the HindIII/SacI fragment of BHUM1962 carrying the *PGK1* promoter. BHUM1962 was generated by a combination of three fragments: (*i*) the SacI/HindIII backbone fragment of BHUM1505, (*ii*) the HindIII/SalI fragment carrying the *PGK1* promoter obtained from BHUM1043 using primers PGK Pr fw and PGK Pr rev, and (*iii*) the SalI/SacI *FLO11* secretion signal from BHUM1879.

Recombinant Overproduction and Crystallization of Epa1A Domains. Both the wild-type Epa1A and all subtype-switched variants were overproduced using the low-temperature protocol developed by Veelders et al. (2). The only modification to the protocol was the use of *Escherichia coli* strain shuffle T7 express (NEB) instead of *E. coli* Origami 2, slightly improving yields. After lysis and clarification of the supernatant, the protein was purified by Ni-NTA affinity chromatography (Qiagen) and subsequent size exclusion chromatography, using Superdex 200 prep grade material (GE Healthcare), initially in AM buffer (20 mM Tris·HCl, pH 8.0, 200 mM NaCl). Epa1A interacted strongly with the Superdex 200 material under these conditions, resulting in very poor yields. This issue could be solved by adding either 50 mM lactose (AML buffer) or 10 mM EDTA (AME buffer) to the AM buffer.

Initial crystal screening was performed in a 600-nL sitting-drop setup, using commercially available screens (Qiagen) with a Microsys SQ4000 dispensing system (Genomic Solutions), and yielded several positive conditions at 18 °C. Optimizations of original hits took place in a similar, 96 conditions, 18 °C, 600-nL sitting-drop setup. Finally, optimized hits were reproduced in a 2-μL hanging-drop setup. Drops were composed of 50% (vol/vol) protein solution in AML buffer (6 or 12 mg/mL) and 50% (vol/vol) reservoir solution.

To obtain Epa1A·T-antigen crystals, Epa1A crystals were grown as described above. The crystals were then soaked in mother liquor supplemented with 1 mM EDTA. Crystals underwent this process three times sequentially, for 2 h, 1 h, and 30 min, respectively. Next, crystals were picked again and given into a drop containing mother liquor supplemented with 2 mM T-antigen and 2 mM $CaCl_2$. Crystals were soaked with T-antigen for 2–24 h. All crystals were frozen in mother liquor supplemented with 20% glycerol.

Data Collection and Structure Solution. Datasets for structure solution were recorded at the European Synchrotron Radiation Facility (ESRF) beamlines ID14-2 for Epa1A, ID23-2 for Epa1→3A, and ID14-4 for Epa1→6A. The Epa1A·T-antigen dataset was collected at Bessy II beamline 14.1. Finally, the dataset for Epa1→2A was recorded on a mar345dtb area detector system (Marresearch), using an FR591 rotating anode (Bruker/Nonius, copper target) as X-ray source (Table S1).

The structure of Epa1A was solved via molecular replacement, using a carefully trimmed homology model based on Flo5A generated with the program CHAINSAW (3). The homology model was based on a multiple alignment as published by Veelders et al. (2) and is similar to the one presented in Fig. S1. Subtype-switched Epa1A variants crystallized isomorphously and were solved using the Epa1A structure by molecular substitution and subsequently exchanging the mutated amino acids with Coot (4). The very same process was applied to the Epa1A·T-antigen dataset. Phase solution was performed with PHASER (5); data processing with XDS,

PHENIX, and CCP4 (3, 6, 7); and final refinement with REFMAC5 (8), phenix.refine, and Coot (4) (Table S2).

Secondary structure assignment was performed with STRIDE (9) as shown in Fig. 2. Figures of protein structures were generated with the molecular graphics program PyMol v1.4 (10).

Phylogenetic Analysis. Phylogenetic analysis was performed by the neighbor-joining method, using Clustal X2.0 (11), COBALT, or a local copy of t-coffee implemented with 3DCoffee (12, 13) for structure-based alignments. Preliminary targets were selected with the help of BLAST (14).

High-Throughput Glycan-Binding Assays. The CFG glycan array used consists of different groups of oligosaccharides that are presented by mammalian cells. Recombinant Epa1A domains were fluorescently labeled using an AlexaFluor 488 SPD kit (Invitrogen) and applied to CFG array V4.1 chips at concentrations ranging from 1 μg/mL to 200 μg/mL. Chip surfaces were repeatedly washed and remaining fluorescence was measured and quantified.

Fluorescence Titrations of Epa1A and Variants. Fluorescence titrations were performed in AM buffer, pH 8, which had been supplemented with 1 mM EDTA and 5 mM $CaCl_2$. Five hundred microliters of protein solution (0.3 mg/mL protein in supplemented AM buffer) was titrated against analyte solution containing either lactose or T-antigen.

Tryptophans were excited at a wavelength of 295 nm, and the quench was followed at the emission maximum, which was always observed between 340 and 345 nm. Measurements were done as triplicates, averaged, and fitted with Qtiplot (15), using Eq. **S1**,

$$q(c) = \frac{q_{\max} \cdot c}{K_D + c}, \qquad \textbf{[S1]}$$

where q is quench, $q_{\max}$ is maximum quench, c is ligand concentration, and K_D is dissociation constant.

Adhesion of *S. cerevisiae* to Human Epithelial Cells. For adhesion tests of *S. cerevisiae* to human epithelial cells, strain BY4741 was used, carrying plasmids with the appropriate *P_{PGK1}-3HA-EPAA-FLO11BC* constructs (Table S4). Specifically, different *EPAA*-encoding domains were tagged with a HA epitope and fused to the BC domain of the flocculin gene *FLO11*. They were expressed in *S. cerevisiae* from the *PGK1* promoter.

Detection of EpaA Domains by Fluorescence Microscopy. In a first step, the presence of EpaA domains at the *S. cerevisiae* cell surface was quantified by immunofluorescence microscopy. For this purpose, cultures of plasmid-carrying strains were grown in low fluorescence yeast medium to an optical density at 595 nm of 1, before cells were washed three times in PBS/1% BSA. Then, cells were incubated with a monoclonal mouse anti-HA antibody (H3663; Sigma Aldrich) at a dilution of 1:1,000 in PBS/1% BSA for 30 min at room temperature (RT). After three wash steps, cells were incubated in darkness with a Cy3-conjugated secondary goat anti-mouse antibody (C2181; Sigma Aldrich) at a dilution of 1:10,000 in PBS/1% BSA for 20 min at RT. After three further washing steps, a Zeiss Axiovert 200 M microscope was used to (*i*) visualize *S. cerevisiae* cells with differential interference contrast and (*ii*) detect EpaA domains at the cell surface, using a rhodamine filter set (AHF Analysentechnik). Cells were photographed with a Hamamatsu Orca ER digital camera and pictures were processed and analyzed using the Volocity software (Improvision). Fluorescence signals were then quantified using the ImageJ software (16).

Epithelial Cell Cultures. For EpaA-directed adhesion assays, the human epithelial cell line Caco-2 (American Type Culture Collection HTB-37) was used, which is a continuous line of heterogeneous human epithelial colorectal adenocarcinoma cells. To gain a confluent monolayer, Caco-2 cells were first grown in 75-cm^2 tissue culture flasks (Greiner) and split 1:3 every second or third day, depending on the confluence, which did not exceed 80%. Once the cell culture was initiated, a periodic medium change was performed using Dulbecco's Modified Eagle Medium (DMEM) supplemented with 10% heat-inactivated fetal bovine serum (FBS), 1 mM sodium pyruvate, and 1% gentamicin (Invitrogen). After approximately 20 subcultures, cells were seeded into 24-well polystyrene plates (Greiner) and incubated at 37 °C under 5% CO_2 for 1–2 d until a confluent monolayer was formed.

Adhesion Assay. Adhesion assays of *S. cerevisiae* on human epithelial Caco-2 cell lines were performed as previously described (17). Briefly, 24-well polystyrene plates with a confluent monolayer of Caco-2 cells were used after removal of the culture medium and addition of 250 μL fresh prewarmed DMEM without gentamicin. *S. cerevisiae* strains carrying appropriate plasmids were grown in YPD medium to exponential phase at 30 °C and diluted in DMEM/10% FBS/1 mM sodium pyruvate to a concentration of approximately 6,000 cells per milliliter of medium. Fifty microliters of these yeast cell suspensions were then added to each well with a confluent layer of Caco-2 cells. Plates were incubated at 37 °C under 5% CO_2 for 0, 30, 60, 120, or 180 min, respectively. The complete supernatant containing the nonadherent *S. cerevisiae* cells was removed and plated on YPD agar to determine the colony forming units (cfu). To determine the adherent yeast cells, wells were washed twice with 300 μL phosphate-buffered saline (PBS) before the epithelial cells together with the attached *S. cerevisiae* cells were scratched off the polystyrene surface. The resulting suspension was also plated on YPD plates to determine the cfu of adherent cells. After incubation for 2 d at 30 °C, cfu values for nonadherent and adherent cells were determined using an aCOLyte colony counter (7510 DWS; Synbiosis). The average values for nonadherent and adherent cells were determined on the basis of 10 independent experiments. Outliers were eliminated with the help of the standard deviation, the standard error, and a *t* test. Relative adhesion values (A) were calculated by using the formula A = cfu (adherent cells)/cfu (adherent cells) + cfu (nonadherent cells).

1. Guthrie C, Fink GR (1991) *Guide to Yeast Genetics and Molecular Biology* (Academic, San Diego).
2. Veelders M, et al. (2010) Structural basis of flocculin-mediated social behavior in yeast. *Proc Natl Acad Sci USA* 107:22511–22516.
3. CCP4 (1994) The CCP4 suite: Programs for protein crystallography. *Acta Crystallogr D Biol Crystallogr* 50:760–763.
4. Emsley P, Lohkamp B, Scott WG, Cowtan K (2010) Features and development of Coot. *Acta Crystallogr D Biol Crystallogr* 66:486–501.
5. McCoy A, et al. (2007) Phaser Crystallographic Software. *J Appl Cryst* 40:658–674.
6. Kabsch W (2010) XDS. *Acta Crystallogr D Biol Crystallogr* 66:125–132.
7. Adams PD, et al. (2010) PHENIX: A comprehensive Python-based system for macromolecular structure solution. *Acta Crystallogr D Biol Crystallogr* 66: 213–221.
8. Murshudov GN, Vagin AA, Dodson EJ (1997) Refinement of macromolecular structures by the maximum-likelihood method. *Acta Crystallogr D Biol Crystallogr* 53:240–255.
9. Heinig M, Frishman D (2004) STRIDE: A web server for secondary structure assignment from known atomic coordinates of proteins. *Nucleic Acids Res* 32:W500–W502.
10. Delano WL (2002) *The PyMOL Molecular Graphics System* (DeLano Scientific, San Carlos, CA).
11. Larkin MA, et al. (2007) Clustal W and Clustal X version 2.0. *Bioinformatics* 23: 2947–2948.
12. Notredame C, Higgins DG, Heringa J (2000) T-Coffee: A novel method for fast and accurate multiple sequence alignment. *J Mol Biol* 302:205–217.
13. O'Sullivan O, Suhre K, Abergel C, Higgins DG, Notredame C (2004) 3DCoffee: Combining protein sequences and structures within multiple sequence alignments. *J Mol Biol* 340:385–395.

14. Altschul SF, et al. (1997) Gapped BLAST and PSI-BLAST: A new generation of protein database search programs. *Nucleic Acids Res* 25:3389–3402.
15. Vasilef I (2009) *QtiPlot: Data Analysis and Scientific Visualization* (ProIndep Serv, Romania).
16. Abramoff MD, Magalhaes PJ, Ram SJ (2004) Image processing with ImageJ. *Biophotonics Int* 11:36–42.
17. Dieterich C, et al. (2002) In vitro reconstructed human epithelia reveal contributions of *Candida albicans* EFG1 and CPH1 to adhesion and invasion. *Microbiology* 148: 497–506.

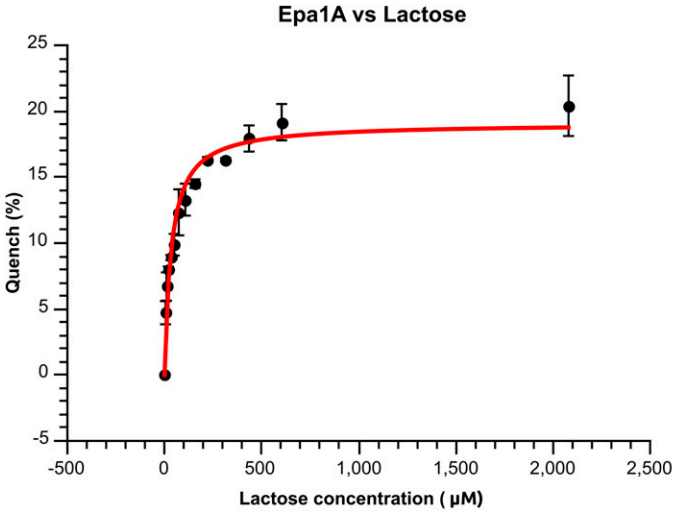

		K_D (μM)	Qmax (%)
β1-4	Epa1A	34.6±6.1	19.1±0.8
	Epa1→2A	128.0±16.3	23.7±0.9
	Epa1→3A	27300±5670	12.8±3.3
	Epa1→6A	33.5±6.6	18.8±0.8
β1-3	Epa1A	2.1±0.3	28.0±0.8
	Epa1→3A	30.0±6.1	16.3±0.9
	Epa1→6A	1.7±0.4	28.6±1.2

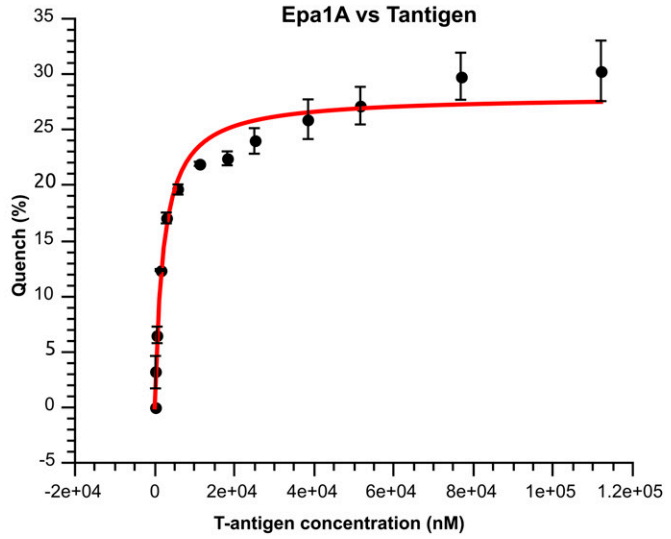

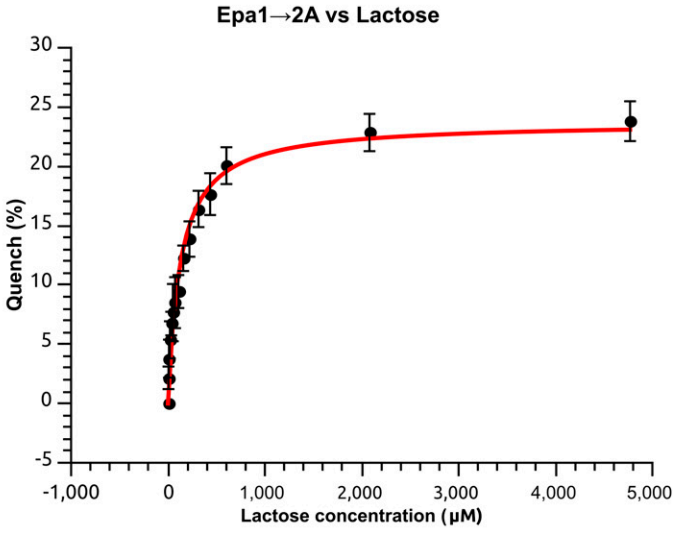

Fig. S1. Examples and table summary for fluorescence titrations of Epa domains against lactose or T-antigen. Several examples are shown for fluorescence titrations, and a summary of dissociation constants (K_D) and maximum quench (Q_{max}) is shown.

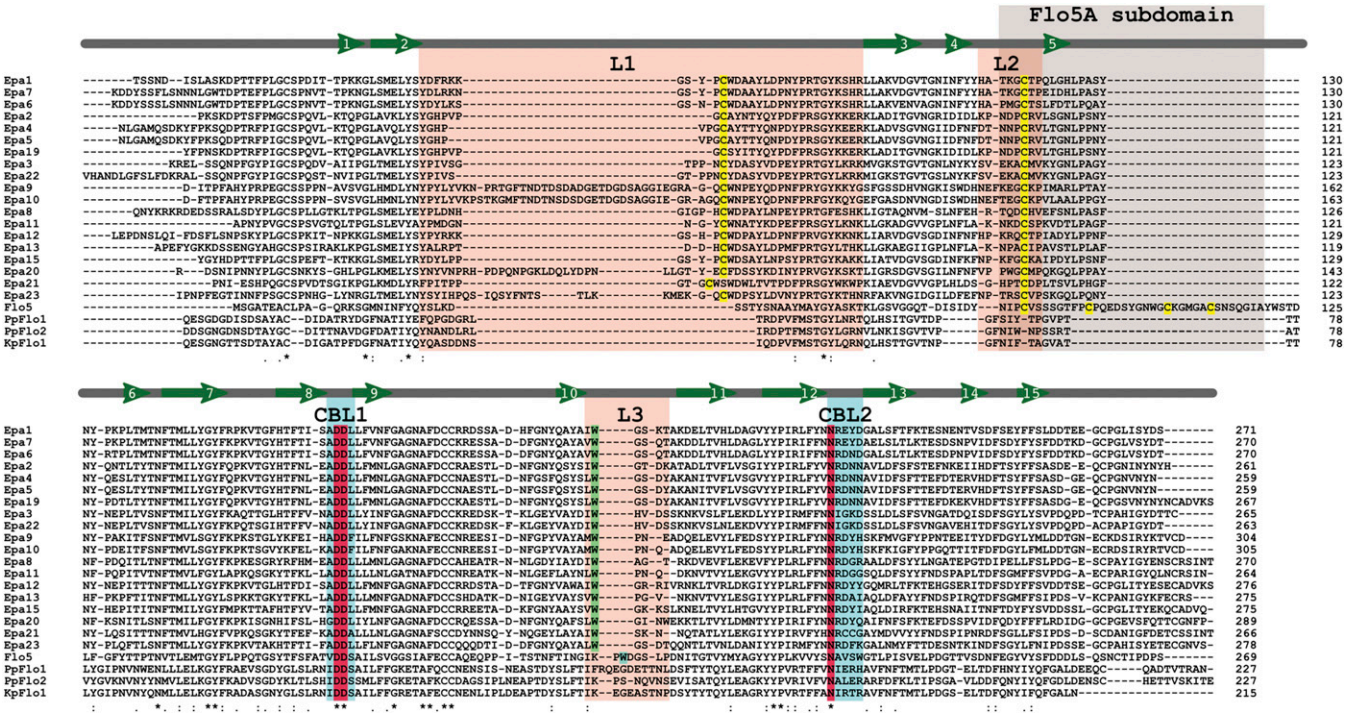

Fig. S2. Structure-based sequence alignment of different PA14/Flo5-like A domains. Shown is sequence alignment of PA14/Flo5-like A domains from *C. glabrata* Epa proteins, *S. cerevisiae* Flo5, and putative adhesins from *Pichia pastoris*/*Komagataella pastoris*. A local copy of t-coffee implemented with 3DCoffee (12, 13) and the 3D structures of Epa1A and Flo5A were used to generate the structure-based sequence alignment. The Epa1A secondary structure is shown over the alignment. The outer binding pocket is composed of the loops L1, L2, and L3, which are highlighted in light red. The inner binding pocket, which is composed of the CBL1 and CBL2 loops, is highlighted in cyan. The *DcisD* motif and N225 of the CBL2 loop, which are complexed to a Ca^{2+} ion for carbohydrate binding, are marked in red. Cysteines conferring disulfide formation are marked in yellow. W198 in L3, which confers galactoside specificity of the inner subpocket of the Epa adhesins, is shown in green. W196 of Flo5 is also in the L3 loop (in green), but is not involved in ligand-binding specificity.

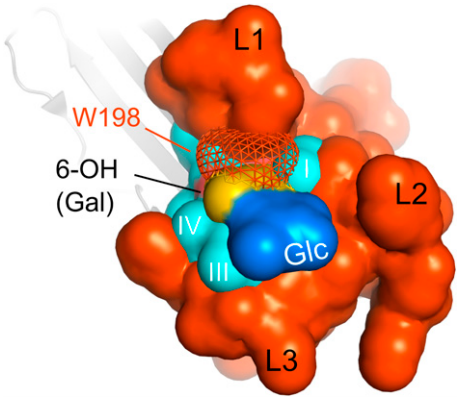

Fig. S3. Epa1A outer binding site. Orange: L loops solvent accessible surface. Cyan: CBL loops solvent accessible surface (I, III, and IV mark visible CBL2 positions). Galactose and glucose are represented in yellow and blue, respectively. Red mesh: surface that is occluded by W198 side chain. Around 50% of the galactose moiety is rendered inaccessible by the presence of the tryptophane, whereas the 6-hydroxyl is still solvent exposed, indicating that modification of galactose, e.g., by sulfate or other glyco-moieties, is possible at this position.

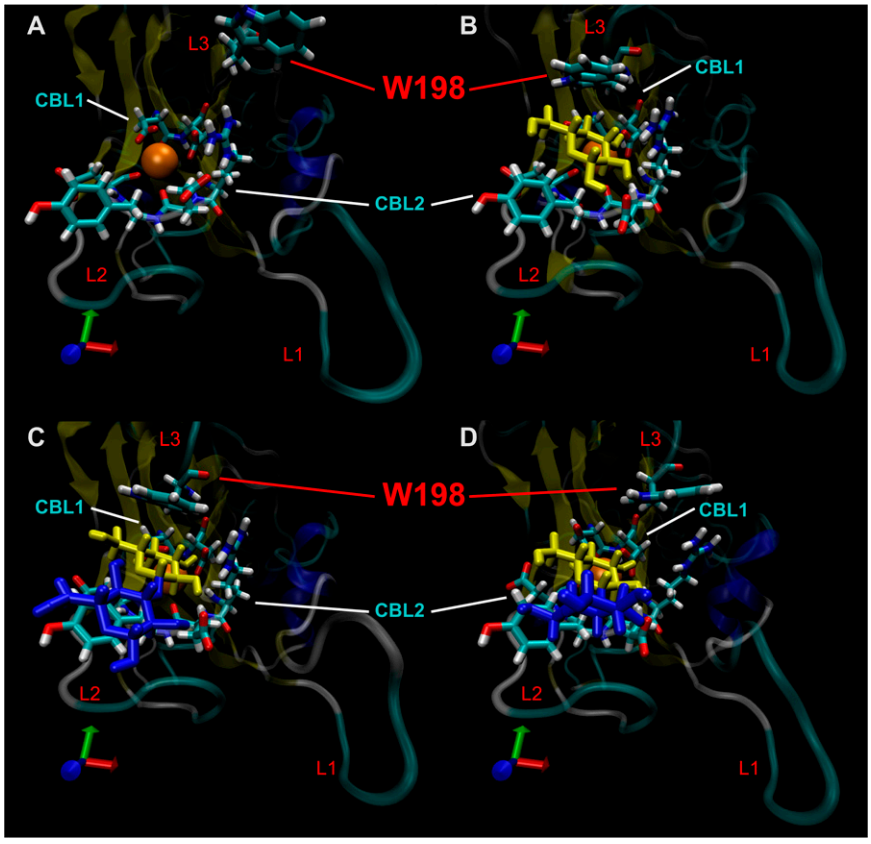

Fig. S4. Molecular dynamics analysis of carbohydrate binding by the Epa1A domain. The Epa1A domain was subjected to molecular dynamics, using AMBER11 with the ff99sb and GLYCAM06 force fields. The Epa1A/Ca^{2+} complex was positioned in a periodic, water-filled and neutralized box either alone (*A*, Movie S1), in complex with galactose (*B*, Movie S2), complexed to Galβ1–3Glc (*C*, Movie S3) or bound to lactose (Galβ1–4Glc; *D*, Movie S4). The box size was chosen as 80 × 62 × 66 Å and the molecular dynamics were performed at 300 K, step size 2 fs, using an isothermal-isobaric ensemble (NPT). After minimization and equilibration for 2 ns, trajectories were collected for a further 18 ns and analyzed with VMD. The figures and movies depict regions of the glycan-binding site crucial for recognition.

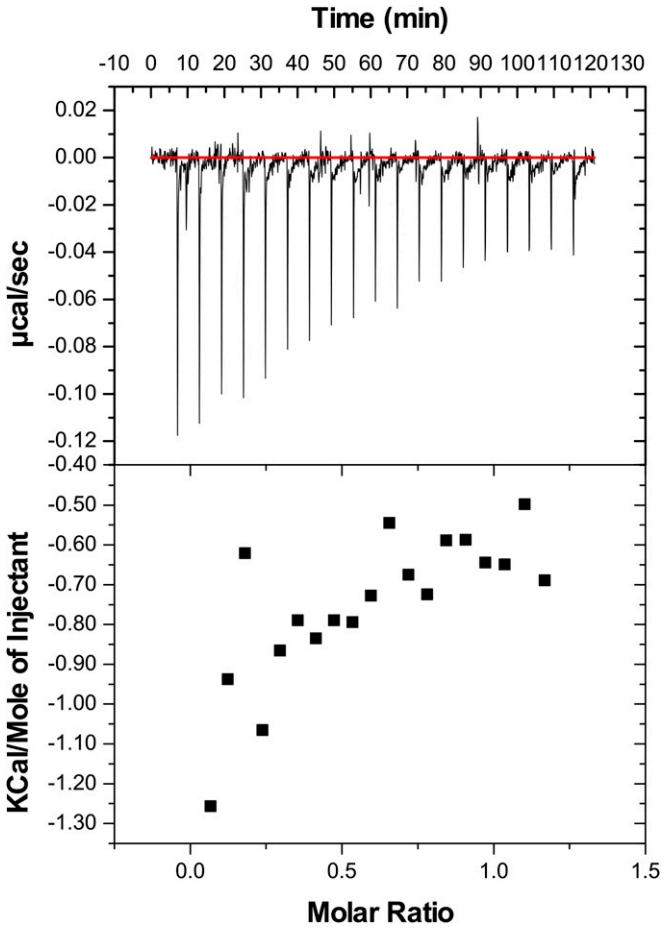

Fig. S5. Epa1A W198A mutant fails to bind T-antigen. (*Upper*) Isothermal titration calorimetric (ITC) data (black) and calculated baseline (red). (*Lower*) Processed data. No fitting values are shown, because the minor heats observed are most consistent with dilution enthalpy. Accordingly, an erroneously assumed 1:1 binding model results in calculated errors ~15 times larger than estimated values for K_D, ΔH, or ΔS.

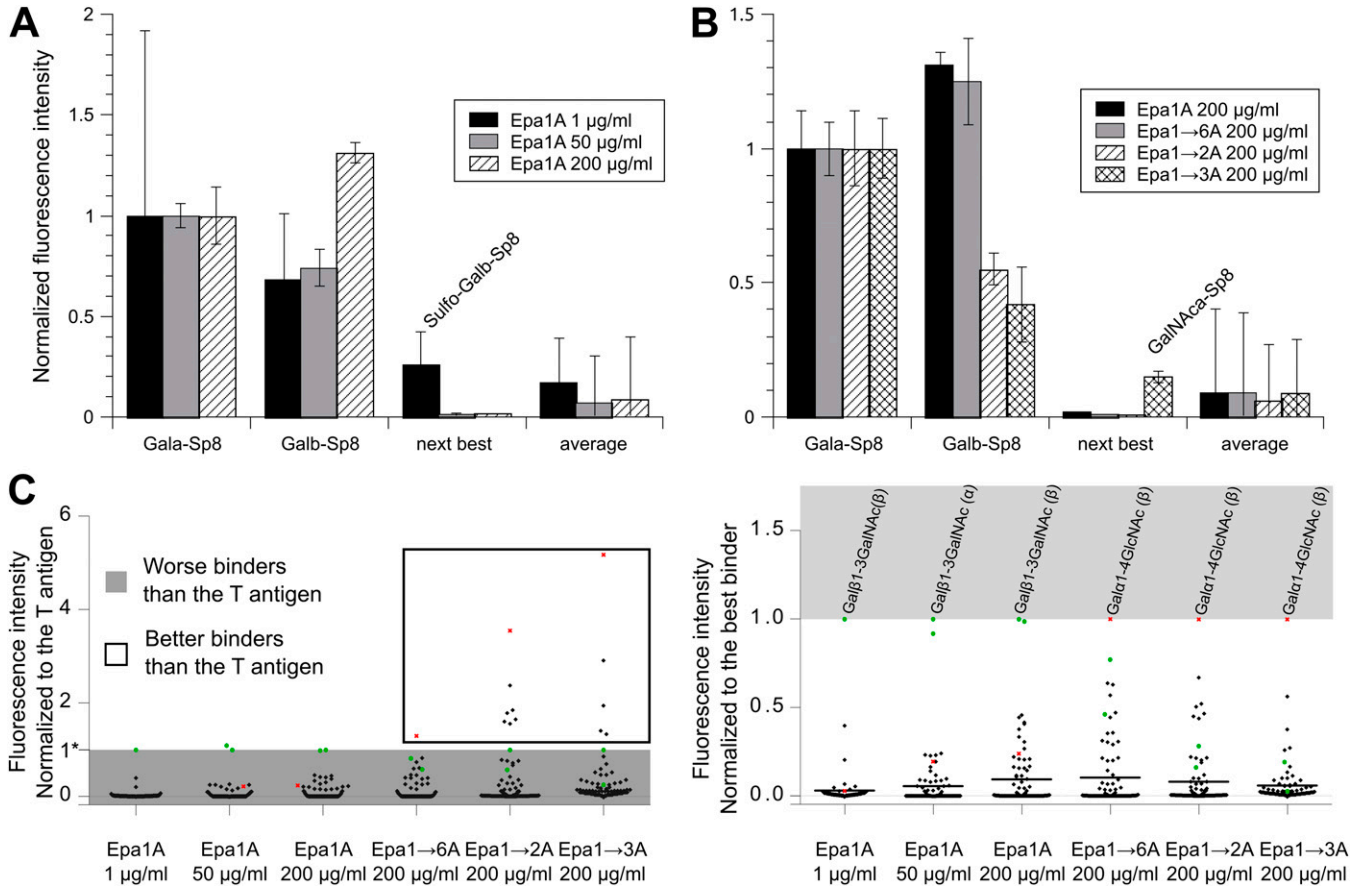

Fig. S6. Binding analysis of Epa1A and cluster-converted variants to CFG array presented mono- and disaccharides. (*A*) Concentration-dependent binding of Epa1A to monosaccharides. Binding intensities have been normalized to Galα-Sp8. Binding was always best for either Galα-Sp8 or Galβ-Sp8. For comparison, the next best ligand intensity is given next. The average intensity of all monosaccharides presented on the array, including both galactose isoforms, is presented on the fourth position. (*B*) Binding of cluster-converted Epa1A variants to monosaccharides. (*C*) Concentration-dependent binding of Epa1A to disaccharides, as well as of subtype-switched Epa1A variants. T-antigen (Galβ1–3GalNAc) and α-*N*-acetyl-lactosamine (Galα1–4GlcNAc) are highlighted as green dots and red dots, respectively. (*Left*) Binding intensities are normalized to the binding to the T-antigen. Overall, Epa1A binds preferentially to the T-antigen, whereas several other binders are better for subtype-switched variants (indicated by a black frame). (*Right*) Binding intensities are normalized to binding to the best binder of each variant to delineate variant-specific promiscuity. Epa1A and Epa1→3A present few, well-defined high binders with many low binders. Epa1→6A and Epa1→2A, on the other hand, show a fairly spread out distribution, indicating a significant degree of promiscuity, and the capacity to bind many different disaccharides without major differences in affinity.

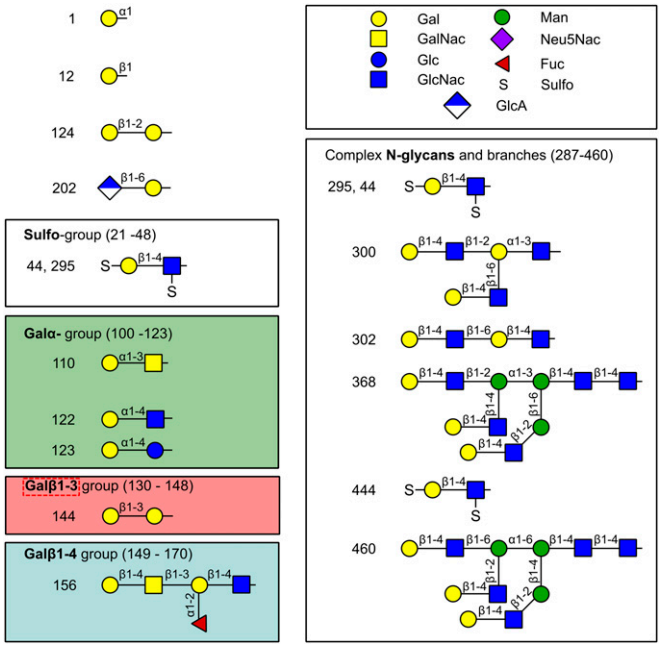

Fig. S7. Best binders for EpaA subtype-switched variants. EpaA subtype-switched variants best binders highlighted in Fig. 4, and not present already in Fig. 1, are presented here in CFG standard notation.

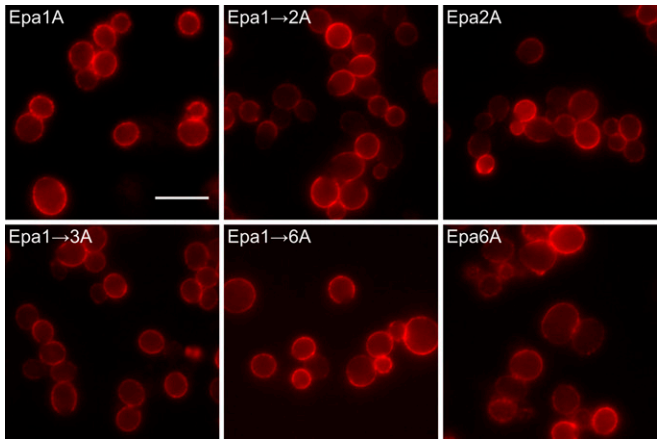

Fig. S8. Presence of different EpaA domains on *S. cerevisiae*. *S. cerevisiae* strain BY4741 carrying BHUM1983 (Epa1A), BHUM1984 (Epa1A→2A), BHUM1985 (Epa2A), BHUM2017 (Epa1A→3A), BHUM2016 (Epa1A→6A), or BHUM2018 (Epa6A) was grown to logarithmic phase and EpaA domains were detected by immunofluorescence microscopy, using anti-HA primary and Cy3-conjugated secondary antibodies. (Scale bar, 10 μm.)

Table S1. Data collection statistics for Epa1A and subtype-switched variants

	Epa1A	Epa1→6A	Epa1→3A	Epa1→2A	Epa1A·T-antigen
X-ray source	ID14-2, ESRF	ID14-4, ESRF	ID23-2, ESRF	Rotating anode (FR591, CuKα)	ID14.1, Bessy II
Wavelength, Å	0.9330	0.9395	0.8762	1.5418	0.9180
Space group	$C222_1$	$C222_1$	$C222_1$	$C222_1$	$C222_1$
Cell parameters, Å					
a	74.64	74.43	75.74	74.56	74.60
b	104.33	103.89	103.53	104.04	103.90
c	69.79	69.28	70.48	69.15	69.40
Resolution, Å	1.50–19.9 (1.50–1.58)	1.55–19.6 (1.55–1.63)	1.90–46.2 (1.90–2.00)	2.00–19.8 (2.00–2.11)	1.24–10.0 (1.24–1.31)
Completeness, %	98.8 (98.7)	99.6 (99.9)	99.5 (99.4)	97.7 (99.7)	98.7 (97.5)
Total reflections	174,640	186,996	115,032	55,079	309,225
Unique reflections	43,249	39,090	22,061	18,024	75,251
Multiplicity	4	4.8	5.2	3.1	4.1
R_{merge} (%)	7.0 (65.5)	4.0 (47.4)	14.5 (49.3)	12.3 (51.9)	3.4 (55.3)
Mean I/σ	14.6 (2.6)	26 (3.5)	7.5 (2.5)	7.4 (2.2)	22.7 (2.7)

Data in parentheses correspond to the highest resolution shell.

Table S2. Refinement statistics for Epa1A and subtype-switched variants

	Epa1A	Epa1→6A	Epa1→3A	Epa1→2A	Epa1A·T-antigen
Resolution, Å	19.9–1.50	19.6–1.55	37.9–1.90	19.6–2.05	10.0–1.24
R_{work}, %	15.7	14.4	16.9	20.4	11.9
R_{free}, %	18.6	17.1	21.7	23.9	15.5
Reflections, all	41,751	37,731	22,056	16,152	72,672
Test set	1,498	1,358	782	571	2,579
No. atoms	2,122	2,089	3,735	2,017	2,484
Water molecules	274	208	160	140	392
B-factor, $Å^2$	18.1	20.6	26.0	17.3	15.0
rms deviations					
Bond length, Å	0.015	0.015	0.014	0.01	0.013
Bond angle, °	1.601	1.571	1.275	1.296	1.524

Table S3. Yeast strains

Strain	Relevant genotype	Source
BY4741	S288c *MATa his3Δ1 leu2Δ0 met15Δ0 ura3Δ0*	Euroscarf
ATCC2001	*C. glabrata* wild-type strain CBS138	www.atcc.org
RH2662	Σ1278b *MATa ura3-52 flo11Δ::kanR*	(1)
WY423	Σ1278b *MATa ura3-52 his3::hisG leu2::hisG 3HA-FLO11*	(2)

1. Braus GH, Grundmann O, Bruckner S, Mosch HU (2003) Amino acid starvation and Gcn4p regulate adhesive growth and FLO11 gene expression in Saccharomyces cerevisiae. *Mol Biol Cell* 14:4272–4284.
2. Guo B, Styles CA, Feng QH, Fink GR (2000) A Saccharomyces gene family involved in invasive growth, cell-cell adhesion, and mating. *Proc Natl Acad Sci USA* 97:12158–12163.

Table S4. Plasmids

Plasmid	Relevant genotype	Source
pET-28(a)+	P_{T7} 6x*His lacI Kan*^{R}	Merck Germany
BHUM0778	P_{FLO11}-*FLO11*-T_{FLO11} in YCplac33	(1)
BHUM1043	P_{PGK1}-*FLO11*-T_{PGK1} in YEplac181	(2)
BHUM1327	P_{FLO11}-*FLO11*$^{(aa1–25)}$-*FLO11*$^{(aa214–1,360)}$-T_{FLO11} in YCplac33	(3)
BHUM1505	P_{FLO11}-*FLO11*$^{(aa1–24)}$-*FLO5*$^{(aa272–1,075)}$-T_{FLO11} in YCplac33	(3)
BHUM1601	P_{FLO11}-*FLO11*$^{(aa1–30)}$-3HA-*FLO11*$^{(aa31–1,360)}$-T_{FLO11} in YCplac33	This study
BHUM1760	P_{FLO11}-*FLO11*$^{(aa1–30)}$-3HA-*FLO11*$^{(aa214–1,360)}$-T_{FLO11} in YCplac33	This study
BHUM1804	*EPA1*$^{(aa31–271;E220D;Y221N;D222N)}$ in pET-28a(+)	This study
BHUM1805	*EPA1*$^{(aa31-271;R219I,E220G;Y221K)}$ in pET-28a(+)	This study
BHUM1806	*EPA1*$^{(aa31–271;E220D;Y221N)}$ in pET-28a(+)	This study
BHUM1829	*EPA1*$^{(aa31–271)}$ in pET-28a(+)	This study
BHUM1835	P_{FLO11}-*FLO11*$^{(aa1–30)}$-3HA-*EPA1*$^{(aa31–271)}$-*FLO11*$^{(aa214–1,360)}$-T_{FLO11} in YCplac33	This study
BHUM1836	P_{FLO111}-*FLO11*$^{(aa1–30)}$-3HA-*EPA1*$^{(aa31–271;R219I,E220G;Y221K)}$-*FLO11*$^{(aa214–1,360)}$-$T_{FLO11}$ in YCplac33	This study
BHUM1871	P_{FLO11}-*FLO11*$^{(aa1–30)}$-3HA-*EPA2*$^{(aa32–262)}$-*FLO11*$^{(aa214–1,360)}$-T_{FLO11} in YCplac33	This study
BHUM1877	P_{FLO11}-*FLO11*$^{(aa1–30)}$-3HA-*EPA6*$^{(aa26–271)}$-*FLO11*$^{(aa214–1,360)}$-T_{FLO11} in YCplac33	This study
BHUM1879	*SalI-20bp-FLO11*$^{(aa1–25)}$-*SacII-GCA-SacI* in "pANY-Amp"	Mr Gene
BHUM1889	P_{FLO11}-*FLO11*$^{(aa1–30)}$-3HA-*EPA1*$^{(aa31–271;E220D;Y221N;D222N)}$-*FLO11*$^{(aa214–1,360)}$-$T_{FLO11}$ in YCplac33	This study
BHUM1892	P_{FLO11}-*FLO11*$^{(aa1–30)}$-3HA-*EPA1*$^{(aa31–271;E220D;Y221N)}$-*FLO11*$^{(aa214–1,360)}$-$T_{FLO11}$ in YCplac33	This study
BHUM1962	P_{PGK1}-*FLO11*$^{(aa1–25)}$-*FLO5*$^{(aa272–1,075)}$-T_{FLO5} in YCplac33	This study
BHUM1964	P_{PGK1}-*FLO11*$^{(aa1–25)}$-*FLO11*$^{(aa214–1,360)}$-T_{FLO11} in YCplac33	This study
BHUM1983	P_{PGK1}-*FLO11*$^{(aa1–30)}$-3HA-*EPA1*$^{(aa31–271)}$-*FLO11*$^{(aa214–1,360)}$-T_{FLO11} in YCplac33	This study
BHUM1984	P_{PGK1}-*FLO11*$^{(aa1–30)}$-3HA-*EPA1*$^{(aa31–271;E220D;Y221N;D222N)}$-*FLO11*$^{(aa214–1,360)}$-$T_{FLO11}$ in YCplac33	This study
BHUM1985	P_{PGK1}-*FLO11*$^{(aa1–30)}$-3HA-*EPA2*$^{(aa32–262)}$-*FLO11*$^{(aa214–1,360)}$-T_{FLO11} in YCplac33	This study
BHUM1990	P_{PGK1}-*FLO11*$^{(aa1–25)}$-*EPA3*$^{(aa28–266)}$-*FLO11*$^{(aa214–1,360)}$-T_{FLO11} in YCplac33	This study
BHUM2016	P_{PGK1}-*FLO11*$^{(aa1–30)}$-3HA-*EPA1*$^{(aa31–271;R219I,E220G;Y221K)}$-*FLO11*$^{(aa214–1,360)}$-$T_{FLO11}$ in YCplac33	This study
BHUM2017	P_{PGK1}-*FLO11*$^{(aa1–30)}$-3HA-*EPA1*$^{(aa31–271;E220D;Y221N)}$-*FLO11*$^{(aa214–1,360)}$-$T_{FLO11}$ in YCplac33	This study
BHUM2018	P_{PGK1}-*FLO11*$^{(aa1–30)}$-3HA-*EPA6*$^{(aa26–271)}$-*FLO11*$^{(aa214–1,360)}$-T_{FLO11} in YCplac33	This study

1. Braus GH, Grundmann O, Bruckner S, Mosch HU (2003) Amino acid starvation and Gcn4p regulate adhesive growth and FLO11 gene expression in Saccharomyces cerevisiae. *Mol Biol Cell* 14:4272–4284.
2. Volschenk H, et al. (1997) Engineering pathways for malate degradation in Saccharomyces cerevisiae. *Nat Biotechnol* 15:253–257.
3. Veelders M, et al. (2010) Structural basis of flocculin-mediated social behavior in yeast. *Proc Natl Acad Sci USA* 107:22511–22516.

Table S5. Primers

Primers	Sequence 5′→3′
Mutagenesis	
pET28_Epa1→6A Fwd	ccctattaggttattttataataacagagataatgatggcgcgctcagttttac
pET28_Epa1→6A Rev	gtaaaactgagcgcgccatcattatctctgttattataaaataacctaataggg
pET28_Epa1→2A Fwd	ccctattaggttattttataataacagagataataatggtgcgctcagttttac
pET28_Epa1→2A Rev	gtaaaactgagcgcaccattattatctctgttattataaaataacctaataggg
pET28_Epa1→3A Fwd_1	ccctattaggttattttataataacataggatatgatggcgcactcagttttac
pET28_Epa1→3A Fwd_1	gtaaaactgagtgcgccatcatatcctatgttattataaaataacctaataggg
pET28_Epa1→3A Fwd_2	ccctattaggttattttataataacataggaaaggatggcgcgctcagttttac
pET28_Epa1→3A Rev_2	gtaaaactgagcgcgccatcctttcctatgttattataaaataacctaataggg
Cloning	
fwd-Epa1-aa31	ccatatgacatcttccaatgatatcag
rev-Epa1-aa271	actcgagttaagaagaatcgtagctg
HUM193	ccggaattcgtggcgcggtgccaatactaccggtacttg
HUM194	acgcgtcgacccccaattcaagaatacaattacttagcgtgg
1601-A2-SacI-SacII	aaagagctcccgcgggaaggaggggatccactag
Flo11-5	aaagagctcatagattgtgacaacaattgtgctccagtacc
PGK Pr fw	aaaaagcttatcttgttttgcaagtaccactg
PGK Pr rev	aaagtcgacgttttatatattgttgtaaaaagtagataattacttcc
Epa_1.2_SacII	aaaccgcggacatcttccaatgatatcag
Epa_1.2_SacI	aaagagctcagaagaatcgtagctg
Epa_2_SacII	aaaccgcggcctaaatccaaggatc
Epa_2_SacI	aaagagctcgcagtggtagttatag
Epa_3.2_SacII	aaaccgcggaagcgagaattaagttccc
Epa_3_SacI	aaagagctccctgcatgtagtatcg
Epa_6,7_SacII	aaaccgcggaaggatgactattcttcc
Epa_6,7_SacI	aaagagctccgaagtatcataactaac
SalI-SS-3HA-EpaXA	aaagtcgacatgcaaagaccatttccattcgc

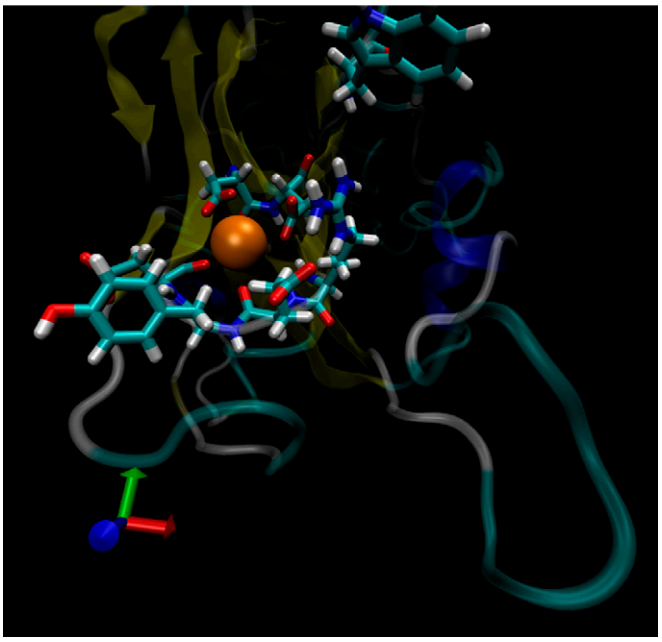

Movie S1. Molecular dynamics simulation of the Epa1A/Ca^{2+} complex without carbohydrate ligand. The Epa1A domain was subjected to molecular dynamics, using AMBER11 with the ff99sb and GLYCAM06 force fields. The Epa1A/Ca^{2+} complex was positioned in a periodic, water-filled and neutralized box alone. The box size was chosen as 80 × 62 × 66 Å and the molecular dynamics were performed at 300 K, step size 2 fs, using an isothermal-isobaric ensemble (NPT). After minimization and equilibration for 2 ns, trajectories were collected for a further 18 ns and analyzed with VMD. The figures and movies depict regions of the glycan-binding site crucial for recognition (Fig. S4).

Movie S1

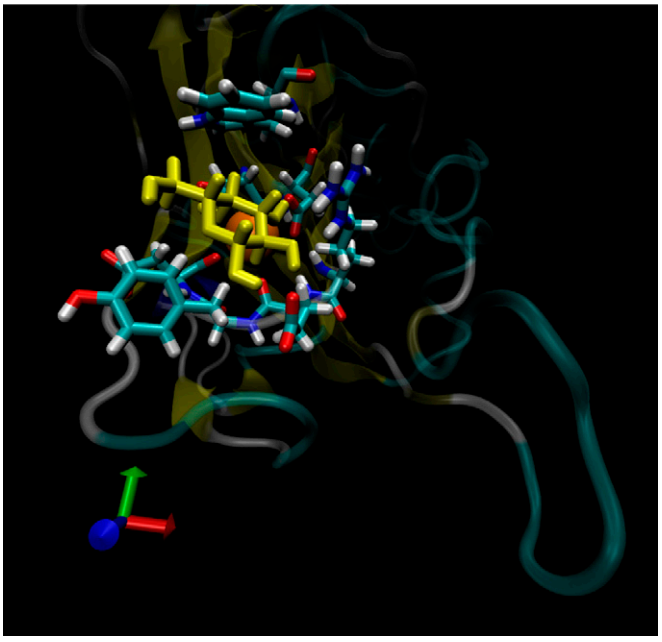

Movie S2. Molecular dynamics of Epa1A/Ca^{2+} complexed with galactose. Epa1A/Ca^{2+}, in complex with galactose, was treated as in Movie S1.

Movie S2

Movie S3. Molecular dynamics of Epa1A/Ca^{2+} complexed with Galβ1–3Glc. Epa1A/Ca^{2+}, in complex with Galβ1–3Glc, was treated as in Movie S1.

Movie S3

Movie S4. Molecular dynamics of Epa1A/Ca^{2+} complexed with lactose. Epa1A/Ca^{2+}, in complex with lactose (Galβ1–3Glc), was treated as in Movie S1.

Movie S4